DRAFT VERSION NOVEMBER 19, 2012
Preprint typeset using LaTeX style emulateapj v. 08/22/09

MODELING THE DISTRIBUTION OF Mg II ABSORBERS AROUND GALAXIES USING BACKGROUND GALAXIES & QUASARS

R. BORDOLOI[1], S. J. LILLY[1], G. G. KACPRZAK[2,3] & C. W. CHURCHILL[4]

Draft version November 19, 2012

ABSTRACT

We present joint constraints on the distribution of Mg II absorption around high redshift galaxies that are obtained by combining two orthogonal probes, the integrated Mg II absorption seen in stacked background galaxy spectra and the distribution of parent galaxies of individual strong Mg II systems as seen in the spectra of background quasars. We present a suite of models that can be used to predict, for different two and three-dimensional distributions, how the projected Mg II absorption will depend on a galaxy's apparent inclination, the impact parameter b and the azimuthal angle between the projected vector to the line of sight and the projected minor axis. The models are all constrained to have the same average projected radial profile, characterized by a b^{-1} power-law with an exponential cut-off at R_{cut} = 37.5 kpc. In general, we find that variations in the absorption strength with azimuthal angles provide much stronger constraints on the intrinsic geometry of the Mg II absorption than the dependence on the inclination of the galaxies. In addition to the clear azimuthal dependence in the integrated Mg II absorption that we reported earlier in Bordoloi et al (2011), we show that strong equivalent width Mg II absorbers ($W_r(2796) \geq 0.3$ Å) are also asymmetrically distributed in azimuth around their host galaxies: 72% of the absorbers in Kacprzak et al (2011), and 100% of the close-in absorbers within 38 kpc of the center of their host galaxies, are located within 50° of the host galaxy's projected semi minor axis. It is shown that either composite models consisting of a simple bipolar component plus a spherical or disk component, or a single highly softened bipolar distribution, can well represent the azimuthal dependencies observed in both the stacked spectrum and quasar line datasets within 40 kpc. Simultaneously fitting both data sets, we find that in the composite model the bipolar cone has an opening angle of $\sim 100°$ (i.e. confined to within 50° of the disk axis) and contains about 2/3 of the total Mg II absorption in the system. The single softened cone model has an exponential fall off with azimuthal angle with an exponential scale length in opening angle of about 45°. We conclude that the distribution of Mg II gas at low impact parameters is not the same as that found at high impact parameters. Mg II absorption within 40 kpc primarily arises from cool Mg II gas entrained in star formation driven winds. At larger impact parameters beyond 40 kpc, there is evidence for a much more symmetric distribution, significantly different from that closer in to the galaxies. At larger radii, a significant component appears which is aligned more with the disk and is possibly inflowing, perhaps as part of a galactic fountain or the inflow of material from further out in the system.

Subject headings: galaxies: evolution: general—galaxies: high-redshift—intergalactic medium—ISM: jets and outflows— quasars: absorption lines

1. INTRODUCTION

The absorption line systems observed in the spectra of background sources such as quasars and galaxies are tracers of the otherwise invisible gaseous structures around galaxies. Combining such absorption-line observations with information on their host galaxies, provide a unique and powerful means to understand the baryonic processes in and around galaxies.

The Mg II $\lambda\lambda$ 2796, 2803 doublet is one of the most studied tracers of the gaseous environment around galaxies. These absorption lines are believed to originate in photo ionized gas at temperatures of around T $\sim 10^4$ K (Bergeron & Stasińska 1986; Charlton et al. 2003) and to trace a wide range of neutral hydrogen column densities of $N_{HI} \sim 10^{16}$- $10^{22} cm^{-2}$ (Churchill et al. 2000; Rigby et al. 2002; Rao et al. 2006) within a few hundred kpc of their host galaxies.

Electronic address: rongmonb@phys.ethz.ch
[1] Institute for Astronomy, ETH Zürich, Wolfgang-Pauli-Strasse 27, 8093, Zürich, Switzerland
[2] Swinburne University of Technology, Victoria 3122, Australia
[3] Australian Research Council Super Science Fellow
[4] New Mexico State University, Las Cruces, NM 88003

There have been many detailed studies on the distribution of column densities, the redshift evolution of number densities and the kinematic signatures of Mg II absorbers using quasar absorption line systems (see e.g. Lanzetta et al. 1987; Sargent et al. 1988; Petitjean & Bergeron 1990; Steidel & Sargent 1992; Charlton & Churchill 1998; Nestor et al. 2005; Prochter et al. 2006). The association of strong Mg II absorption with normal, bright, field galaxies is by now well established (e.g. Churchill et al. 2005 and references herein). The Mg II gas around galaxies is traced out to ~ 100 kpc with absorber covering fractions of 50-80% (Kacprzak et al. 2008; Chen et al. 2010; Nielsen et al. 2012). The anti-correlation between absorber equivalent width and impact parameter is also now well established by several studies (Steidel 1995; Bouché et al. 2006; Chen et al. 2010; Kacprzak et al. 2011b; Bordoloi et al. 2011).

While the association of Mg II absorption with galactic haloes has been secure for some time, the origin and fate of this gas has been less clear. Possibilities have included outflowing material entrained in star-formation driven winds (Weiner et al. 2009; Rubin et al. 2010) or inflowing material feeding the disks of galaxies (Rubin et al. 2012; Martin et al. 2012).

The process of large scale outflows driving cold gas out of the galaxy and polluting the circum-galactic medium (CGM) is certainly a complex one. Moreover, the kinematics and the distribution of cold gas entrained in such star formation driven outflows still remain uncertain (Veilleux et al. 2005). The mechanical energy generated by supernovae explosions and cosmic rays etc. create hot over-pressurized bubbles which sweep up the surrounding ambient material into dense shell like structures. These shells accelerate as they expand and when the reach the low density CGM, Rayleigh-Taylor instabilities set in, which leads to fragmentation of these shells in the CGM (Heckman 2002; Fujita et al. 2009). Although the physical processes involved in such a scenario are likely to be complex, it is likely that cold pockets of gas will be entrained in such outflowing material. Moreover, new clumps of cold gas might form due to thermal instabilities in the hot gas (Fujita et al. 2009). Of course, entrained material can also later fall back onto the galaxy due to gravity (Oppenheimer et al. 2010). Moreover, derived constraints on mass, energetics or momentum of the outflow are hindered with orders of magnitude uncertainties (Prochaska et al. 2011 and references therein). Even idealized outflow models (Fujita et al. 2009) are not well constrained. The opening angle of the outflowing gas, the acceleration of the gas as a function of galactocentric radius, optical depth, covering fraction, density, temperature or the spatial extent of such outflowing gas are all quite uncertain. For more complex models, where the Mg II absorption occurs due to combination of outflowing gas with extended galactic disk or inflowing gas, the fractional contribution from each component also remain unconstrained.

Recently, several studies have sought to infer the distribution of Mg II absorption around galaxies so as to provide diagnostic information on the origin of the enriched material and to try to constrain possible models. Using very large numbers of about 5000 background galaxy spectra from zCOSMOS (Lilly et al. 2007) to probe the profiles of Mg II absorption around 4000 foreground galaxies at $0.5 < z < 0.9$, Bordoloi et al. (2011) showed that the strength of the Mg II absorption was much higher for blue star-forming galaxies than for red, more passive, galaxies, at the same stellar mass. Furthermore, they showed that for inclined foreground disk galaxies, the Mg II absorption is significantly enhanced along the galaxy projected minor axis, at least out to 40-50 kpc from the galaxy. This result indicated that the Mg II absorption must be primarily originating in a bipolar structure aligned with the disk axis, suggesting that it is part of a bipolar outflow driven by star formation.

On the other hand, Kacprzak et al. (2011b) found an anti-correlation between Mg II absorber strength and disk inclination i, as normalized by the impact parameter b, in the sense that the equivalent width of Mg II was anti-correlated with b/i. This was interpreted as being due to co-planner geometry of the absorbers. In parallel Bouche et al. (2011), using the sample of ten $z \sim 0.1$ absorbers of Kacprzak et al. (2011a) found a bimodal distribution of azimuthal angles, 60% of their absorbers being within 30° of the galaxy minor axis. They also interpret their result as to support the bipolar wind scenario. Kacprzak et al. (2012), using 88 $W_r(2796) \geq 0.1$ Å absorbers and 35 $W_r(2796) \leq 0.1$ Å non-absorbers also reported a bimodal distribution of azimuthal angles: They found that the equivalent width distribution for Mg II absorption along the disk major axis are likely skewed towards the weak absorbers than those along the disk minor axis. (Also see Churchill et al. (2012), who find the same result using 51 galaxies with sensitivities to $W_r(2796) \geq 0.003$ Å.

The observational material presented in Bordoloi et al. (2011) and in the studies of Kacprzak et al. (2011b) and Bouche et al. (2011) are in many ways orthogonal. The integrated approach using stacked galaxy spectra measures the *total* Mg II absorption, integrated over all equivalent widths, in some location relative to the host galaxies. This location can be defined over a range of impact parameters b and/or azimuthal angles ϕ (which we throughout the paper define to be relative to the projected minor axis). By stacking the spectra to detect the absorption signal in the first place, this total Mg II absorption is by construction measured as an average over some potentially large sample of foreground galaxies that can be constructed as desired in terms of their luminosities, colors, masses, star-formation rates, apparent inclinations and so on.

In contrast, the quasar line approach involves identifying absorption systems above some individual equivalent width threshold, and then identifying the host galaxies and determining both the location of the quasar line of sight relative to them, and any properties of the host galaxies of interest (colors, star-formation rates etc.). The distribution of these measurements relative to what would have been expected from a sample of galaxies without the Mg II selection can then give information on the Mg II itself. A specific example will make the distinction clear. In the stacked approach, one measures directly the total average Mg II absorption strength as a $f(\phi)$ around galaxies. In the quasar-line approach, one measures the observed distribution of $N(\phi)$ for the hosts of detected Mg II systems and compares this with what would be expected from the general population, i.e. in this case, a flat distribution in $N(\phi)$.

The main aim of the current paper is to critically examine the information that comes from both the integrated spectra approach and the quasar-line approach to see if they present a consistent picture for the distribution of Mg II around galaxies. Then, since we find that they are indeed consistent, we wish to undertake a joint analysis, using both data sets, to define, as well as possible, the global characteristics of this distribution. For both purposes, we need a clear understanding of the role of the inclination of a galaxy in determining the Mg II absorption as seen projected onto the plane of the sky. We therefore construct an extensive suite of models that can be viewed from any angle and with any impact parameter.

The layout of this paper is as follows. In Section 2 we first discuss the construction of simple geometric models for Mg II around galaxies, including the computation of an integrated equivalent width and the definition of the spatial distributions and geometries of the different models that are considered for the simulations. In Section 3 we "observe" these models over the full range of impact parameter b, inclination i, and azimuthal angle ϕ, both to identify the most powerful diagnostics for the geometry and to provide predictions for the run of absorption strength with these observable quantities that can be used to compare with the observations. In Section 3.2 we compare these model predictions to the stacked integrated Mg II measurements, including considering straightforward superposition of different components. In Section 4 the model predictions are compared with the quasar absorption line data, yielding similar results. In section 5, we perform a joint analysis of both the datasets to derive our globally preferred model. Our findings are summarized in Section 6.

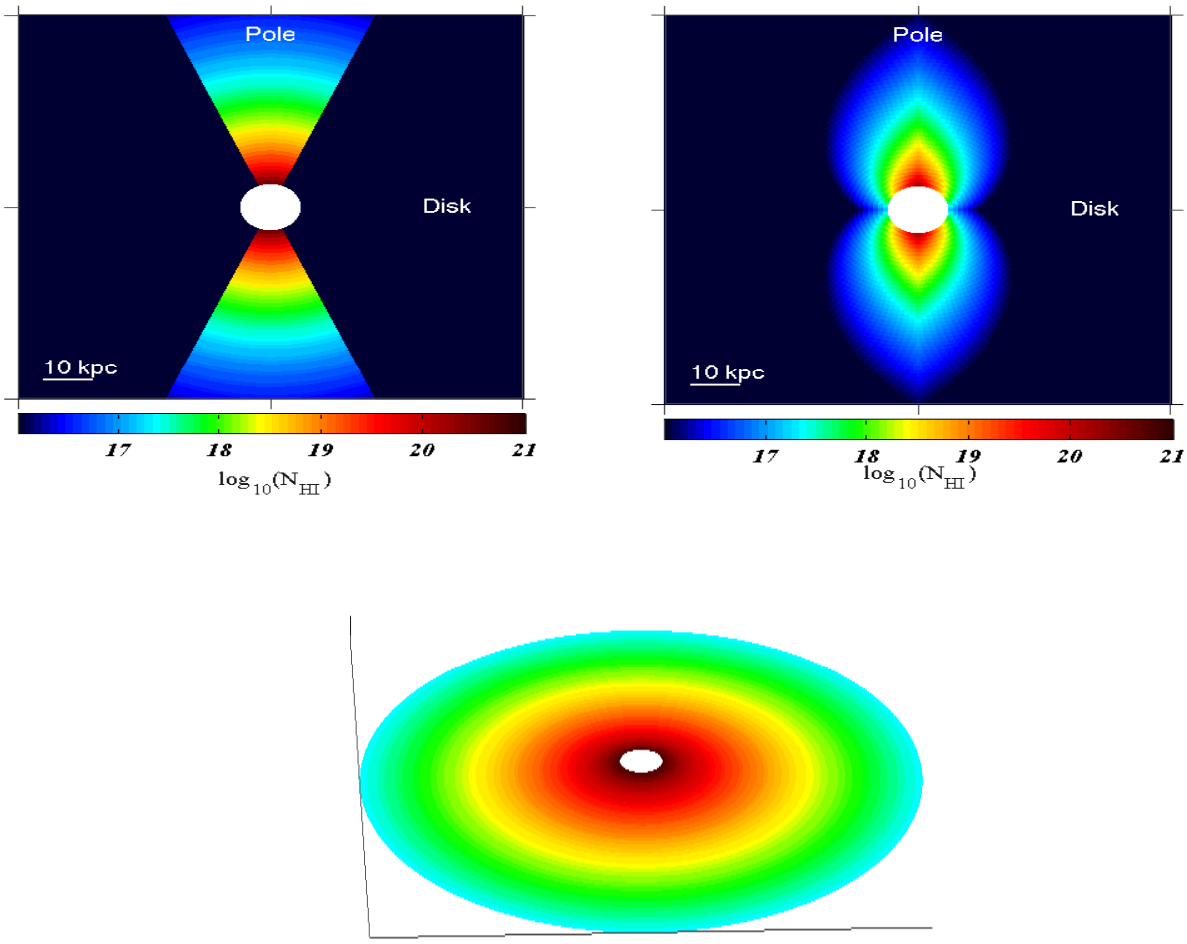

FIG. 1.— *Top panel:* Cross section of the N_{HI} density distribution (in the plane of the sky) for the sharp bipolar cone (top left) and for the softened bipolar cone model (top right) both with an opening angle of 45° viewed edge on. *Bottom panel:* The projected N_{HI} column density distribution for a 2D disk viewed at an inclination angle. For all three cases, the models have the same projected radial profile, with R_{cut} = 37.5 kpc.

Throughout this paper, we adopt a ΛCDM cosmology with $\Omega_m = 0.27$, $\Omega_\Lambda = 0.73$ and $H_0 = 70\ km\ s^{-1}\ Mpc^{-1}$.

2. THE MODEL

We will assume throughout the paper that the light from the galaxy is in a disk and that the ellipticity of this light indicates the inclination of the disk. We describe this orientation by the direction of the pole of this disk, which lies in the direction $\vec{P}$. We then create a set of galaxy models that are each based on a particular 3-dimensional distribution for the absorbing gas that is given in terms of a density $n(\vec{R})$ which is the number density of the neutral hydrogen gas (number of atom per cm^{-3}) in the galaxy at position $\vec{R}$. The angle subtended by $\vec{R}$ with respect to the polar axis $\vec{P}$ is defined to be ψ, i.e. $\cos\psi = \vec{R}.\vec{P}$. We consider a spherically symmetric distribution, a bipolar distribution and a two-dimensional disk. In each case the density distribution is assumed to be rotationally symmetric about the pole.

The galaxy is then rotated randomly through 10^6 orientations, i.e. so that $\vec{P}$ is uniformly distributed on the unit sphere. The expected Mg II absorption is then calculated by integrating through a given line of sight that passes at a projected separation, i.e. impact parameter, b from the centre of the galaxy. The observed column density $N_{HI}(b)$ at impact parameter b is given as

$$N_{HI}(b) = \int_{LOS} n(\vec{R})\, dl\ . \qquad (1)$$

Each of the 10^6 random orientations is associated with a particular inclination for the observer, where the inclination angle i is defined so that $i = 0°$ corresponds to a face-on galaxy and $i = 90°$ corresponds to an edge-on galaxy whose pole lies in the plane of the sky. The inclination angle i has a probability distribution P(i) di $\sim$ sin(i) di, i.e. more galaxies are edge-on than face-on. For simplicity, the lines of sight are chosen to all lie along a particular line in the sky extending from the center of the galaxy, so that each orientation also corresponds to a projected azimuthal angle ϕ between the projected pole of the galaxy, i.e. the observed minor axis, and the arbitrary vector in the plane of the sky along which the

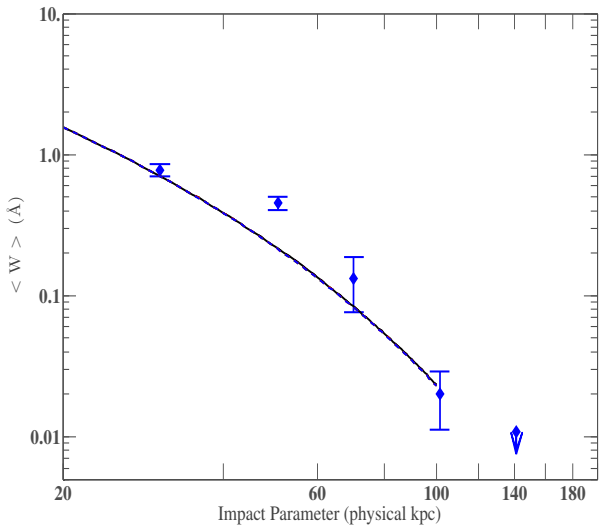

FIG. 2.— The azimuthally averaged radial profile for all models studied in this paper, which are by construction the same. For all models the overall normalization (α) is so chosen that $\langle W_{obs} \rangle \simeq 0.7$ Å within $20 \leq b \leq 50$ kpc. The data points are from Bordoloi et al. (2011).

lines of sight have been calculated. We use $\phi = 0°$ for a sight line that is located along the minor axis, i.e. above the pole of the galaxy, and $\phi = 90°$ corresponds to a sightline aligned along the major axis. This azimuthal angle (ϕ) will be uniformly distributed between $0° \leq \phi \leq 90°$. Throughout this paper, kinematics of the Mg II absorbers are not taken in to account. We quote the total equivalent width of the absorption absorption line system and assume no knowledge of their kinematic velocity spread. All the models will be normalized to the radial profile of blue galaxies from Bordoloi et al. (2011), hence the models studied here will represent blue host galaxies within the stellar mass range of $\sim 10^{9.5} M_{\odot}$ to $10^{10} M_{\odot}$.

For comparison with other works, we ran the models using neutral hydrogen number densities, $n(HI)$ and column densities N_{HI}. For a given galaxy orientation, we then convert the integrated column density $N_{HI}(b)$ to an observed equivalent width in Mg II, $W_{obs}(b)$. We take two approaches. First, we adopt the linear expression from Ménard & Chelouche (2009)

$$N_{HI}(W_{obs}) = (2.45 \pm 0.38) \times 10^{19} \left(\frac{0.5 \cdot W_{obs}}{\text{Å}} \right)^{2.08 \pm 0.24} \; cm^{-2} \quad (2)$$

which has no effects of line saturation. It should be noted that the W_{obs} values quoted here are summed over both the components of the Mg II absorption doublet ($W_{obs} = W_{2796} + W_{2803}$). Since we normalize our models to an observed radial profile $W_{obs}(b)$ the use of the HI number density and the adoption of the above conversion factor are simply book-keeping devices which have no impact on our results.

Second, we modify this relation to account for line saturation. The effects of line saturation in the context of our model may be quite complex, depending on the cloud structure of the Mg II absorbing gas. For instance, it would be possible to have saturated discrete clouds (producing saturated line ratios) whose integrated absorption is nevertheless added linearly along the line of sight through the galaxy because the clouds have sufficiently different velocities. The much broader "beam" of studies using background galaxies rather than quasars is also relevant because small clouds could cover the pc^2 area of the quasar beam but not the 10^8 pc^2 beam probed by a background galaxy. For these reasons, we adopt a simple ad hoc prescription for line saturation. Mg II absorption lines become saturated at column densities of $N_{MgII} \approx 10^{-14}$ cm^{-2}, which is at relatively low hydrogen column densities of $N_{HI} > 10^{19}$ cm^{-2} at solar abundance. Therefore we assume, for all lines of sight, that if $W_{obs}(b, i, \phi) \geq 2$ Å as given by equation 2, then that line of sight is probing a system where the effects of saturation are likely to be present. A new modified $W_{obs,s}$ is obtained by drawing from a Gaussian distribution with mean $W_{obs} = 2.0$ Å and standard deviation $\sigma = 0.3$ Å. The values are chosen to more or less approximate the scatter in the data used to estimate equation 2. The extreme values of the new saturated $W_{obs,s}$, which fall below 0.6 Å are redrawn from a uniform random distribution between 0.6 and 2.0 Å. This is chosen so that the saturated systems do not correspond to unnaturally low equivalent widths.

Since the quoted $W_{obs,s}$ values are summed over both components of the Mg II 2796, 2803 doublet, we have to assume a doublet ratio to convert $W_{obs,s}$ to the equivalent of $W_r(2796)$ values. The oscillator strengths of the Mg II absorption doublet lines have a ratio of 2:1 and in the optically thin regime, their equivalent widths will also have a doublet ratio of 2:1. But as the optical depth of the lines increase and the lines become saturated, the equivalent width ratio also approaches 1:1. In observed quasar absorption line systems the doublet ratios indeed vary from 2 to 1 for $W_r(2796) < 0.1$Å. Furthermore, doublet ratio is also a function of impact parameter. In this paper, we only consider strong ($W_r(2796) \geq 0.3$ Å) systems, which will all be saturated. Hence for simplicity we assume a doublet ratio of 1:1, i.e. the $W_r(2796)$ component will have half the value of W_{obs}.

Given the radial profile $\langle W_{obs} \rangle(b)$ for each of the 10^6 orientations, each with their unique (i, ϕ) we can then average these to yield observable quantities including (1) radial profiles $\langle W_{obs} \rangle(b)$, i.e. averaged over i & ϕ, (2) $W_{obs}(i, \phi)$ at a given b, (3) the inclination profile : $\langle W_{obs} \rangle(i)$ for a given b, averaged over ϕ and (4) azimuthal profiles: $\langle W_{obs} \rangle(\phi)$, at given b and averaged over i. This exercise is then repeated for the different geometrical models constructed as described below.

2.1. *3-D bi-cone and sphere models*

The first model is set up by assuming that absorbing gas is distributed with a conical geometry, aligned along the disk rotation axis. Within the galaxy, the angle with respect to the polar axis is defined to be ψ, i.e. $\cos\psi = \vec{R} \cdot \vec{P}$. Within this cone, the number density is given by the galactocentric radius, R, and to be zero outside the cone. The radial dependence is set to be a power-law with an exponential cut-off, since this will give a good match to the average radial profile in Bordoloi et al. (2011).

$$n(R) = \begin{cases} \alpha \left(\frac{R}{R_{cut}} \right)^{\beta} \exp\left(-\frac{R}{R_{cut}} \right), & \text{if } \psi \leq \chi/2 \\ 0, & \text{otherwise} \end{cases} \quad (3)$$

Here χ is the opening angle of the bipolar cone. The generic models defined by equation 3 are hereafter referred to as *sharp bipolar cone* models. This model represents the simple model of bi-conical outflow coming out of a galaxy. We create a suite of models with opening angles $\chi \in [0°, 180°]$. The model

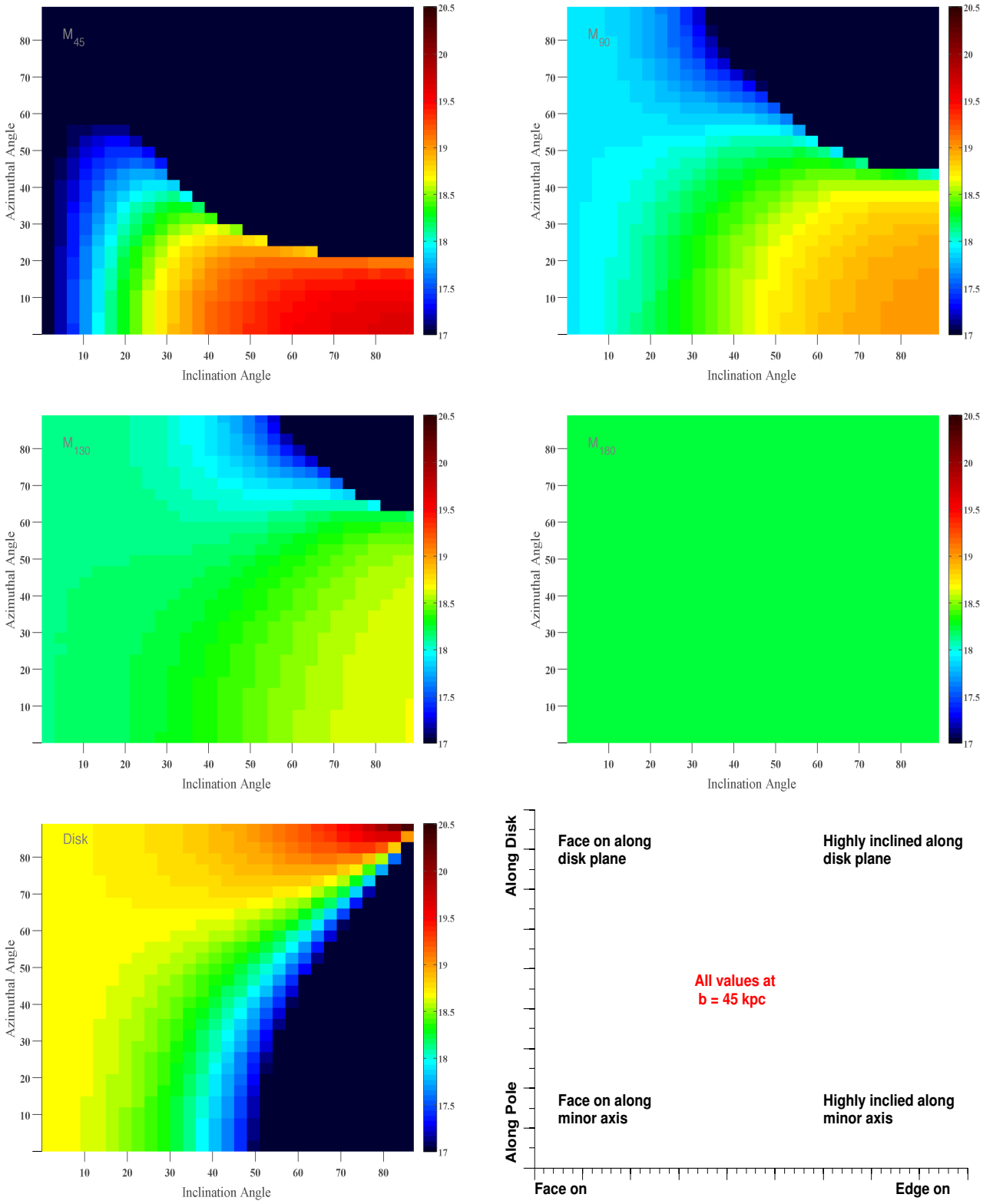

FIG. 3.— The $\log_{10}\langle N_{HI}(b)\rangle$ column density distributions for different models as a function of inclination and azimuthal angle, for $b = 45$ kpc. The models shown here are respectively from top left (i) cone with opening angles (χ) 45°, 90°, 130°, (ii) sphere and (iii) Disk. Different 3-d absorption geometries show clear trends with inclination and azimuthal angles. The last panel shows the orientation of the absorbers.

with $\chi = 180°$ is therefore a full sphere.

We take $\beta = -2.0$ since this will well match the average radial profile in Bordoloi et al. (2011), shown also in figure 3. It is obviously appropriate for a mass-conserving outflow of constant velocity. The default cut-off radius in the exponential (R_{cut}) is set at 37.5 kpc, also to match the average radial

profile. The value of α is set for each of the conical models so that the average $\langle W_{obs} \rangle \simeq 0.7$ Å for $20 \leq b \leq 50$ kpc. This again is chosen to match the observed average radial profile in figure 3. Because the conical models all have the same radial dependence, there is a simple relation between the adopted α and the opening angle χ.

Top left panel of Figure 1 shows a cross section of the N_{HI} column density distribution of the sharp bipolar cone model with $\chi = 45°$ viewed edge on with $i = 0$. For the remainder of the paper we refer to sharp bipolar cone models with a subscript indicating the opening angle χ, i.e. M_{30} has an opening angle of 30° and M_{180} is the sphere.

The second set of bipolar cone models are defined to have the same radial fall-off as previously described, but now with a softened exponential falloff in ψ, i.e.

$$n(R,\psi) = \alpha \left(\frac{R}{R_{cut}}\right)^{\beta} \exp\left(-\frac{R}{R_{cut}}\right) \exp\left(-\frac{2\psi}{\chi}\right) \quad (4)$$

The generic set of models defined by equation 4 are hereafter referred to as *softened bipolar cone* models. Again as before, we set $R_{cut} = 37.5kpc$ and $\beta = -2.0$. The free parameter α is set as before. This model has the feature of a non-zero density down to the plane of the galaxy and might represents a situation in which material also flows back onto the galaxy along the disk plane. The top right panel of figure 1 shows a cross section of the N_{HI} column density distribution in such a model viewed edge on with $\chi = 45°$. $W_{obs}(b)$ is obtained as before using equation 1. We refer to these models as M_{χ}(softened).

Figure 2 shows the averaged radial profiles for four sharp and four softened models (averaged over both inclination and azimuth) compared with the measured radial profile taken from (Bordoloi et al. 2011) (blue data points). By construction, all the models have an identical average radial profile (solid lines). Not surprisingly, the radial profile alone gives no information on the ψ distribution of the absorbing material.

2.2. *2-D disk model*

We also define a 2D model consisting of an infinitesimally thin disk, characterized as

$$N_{perp}(R) = \alpha \left(\frac{R}{R_{cut}}\right)^{-1} \exp\left(-\frac{R}{R_{cut}}\right) \quad ; \text{along the disk} \quad (5)$$

where N_{perp} is column density perpendicular to the disk. The cut-off radius ($R_{cut} = 37.5$ kpc) is identical to that of the 3-D models, but because of the reduced dimensionality, the exponent of the power-law is reduced by one. The normalization term α is again chosen similar to that done in the case of the 3-D models. For the 2-D disk case, the observed column density $N(b)$ can be measured directly without integrating along the line of sight but with a correction for non face-on disks because of the increase path through the disk. The radial position where a line of sight intersects the plane of the disk is given in terms of b, i and ϕ and so, accounting for the longer path length through a inclined disk, we get

$$N(b) = N_{perp} \left(b \left[\sin^2\phi + \left(\frac{\cos\phi}{\cos i}\right)^2 \right]^{1/2} \right) \times \sec i \quad (6)$$

$N(b)$ is converted to $W_{obs}(b)$ using equation 2. The model is again normalized to have $\langle W_{obs} \rangle \simeq 0.7$ within 20 kpc $\leq$ b $\leq$ 50 kpc. The bottom panel of figure 1 shows the *projected* N_{HI} column density distribution of this model viewed at an inclined angle. In figure 2 we over plot the average radial profile for the disk model, which is indistinguishable from that of the 3-D models. As noted above, the average radial profile alone contains no information to distinguish between 2D and 3D geometries.

3. OBSERVABLE QUANTITIES

In this section we describe the basic observable quantities for the different model geometries and diagnose which observables can most efficiently discriminate between them.

3.1. *$N_{HI}(i,\phi)$ column density distribution for different models*

The first observable we focus on is the distribution of absorption column density as a function of i and ϕ at a fixed impact parameter. It can be used to predict the distribution of Mg II-selected galaxies in (i,ϕ) once a threshold is applied in equivalent width and after accounting for the $\sin i$ weighting in random orientations. This is done in section 5.

For the purpose of presentation, we show these in N_{HI} to avoid, for the time being, the question of saturation in Mg II. N_{HI} is computed using equation 2. Figure 3 shows $N_{HI}(i,\phi)$ column densities for a set of sharp cones and the disk model at a fixed impact parameter of $b = 45$ kpc. As expected, the spherical model M_{180} has no variation of absorber strength with inclination and azimuthal angles. For all the other cases both the sharp bipolar cone models and the disk have the strongest absorption for edge on systems with i approaching 90°. However for bipolar cone models, strong systems are preferentially aligned near the minor axis of the galaxies (i.e. $\phi \rightarrow 0°$) whereas for disk models this is reversed and the strongest absorption is aligned along the disk of the galaxy (i.e. $\phi \rightarrow 90°$). It can be seen that all the models, except the completely spherical one, have regions where no absorption occurs. Quasar lines of sight with strong absorption should avoid these regions of (i,ϕ), while lines of sight without strong absorption (e.g. below 0.1 Å) should cluster there, unless small scale clumpiness in the Mg II gas distribution permitted such lines of sight also in regions of much higher average equivalent width.

3.2. *Azimuthal and inclination profiles*

By collapsing one of the angular variables, we can study how N_{HI}, and/or W_{obs} depend on the other angular variable, averaged over some impact parameter range. These profiles can be compared with the observed profiles from the stacked spectra analysis of Bordoloi et al. (2011).

To demonstrate how different model geometry is sensitive to i and ϕ, we consider the models M_{30}, M_{45}, M_{90} and M_{120} as well as the 2-d disk and the sphere (M_{180}) model. For each model W_{obs} and N_{HI} column densities are computed as described in the previous section. We create two observables to compare with the stacked spectra (1) $\langle W_{obs} \rangle$ within $20 \leq b \leq 40$ kpc, averaged over all ϕ, which gives the variation of i within the b bin. (2) $\langle W_{obs} \rangle$ within $20 \leq b \leq 40$ kpc averaged over all i, which gives the average variation of ϕ within the same b bin. Figure 4 shows the variation of $\langle W_{obs} \rangle$ as a function i and ϕ for these six models. The data points are taken from Bordoloi et al. (2011).

The bottom panel shows the azimuthal variation of $\langle W_{obs} \rangle$ where a strong variation is seen. The solid lines show the

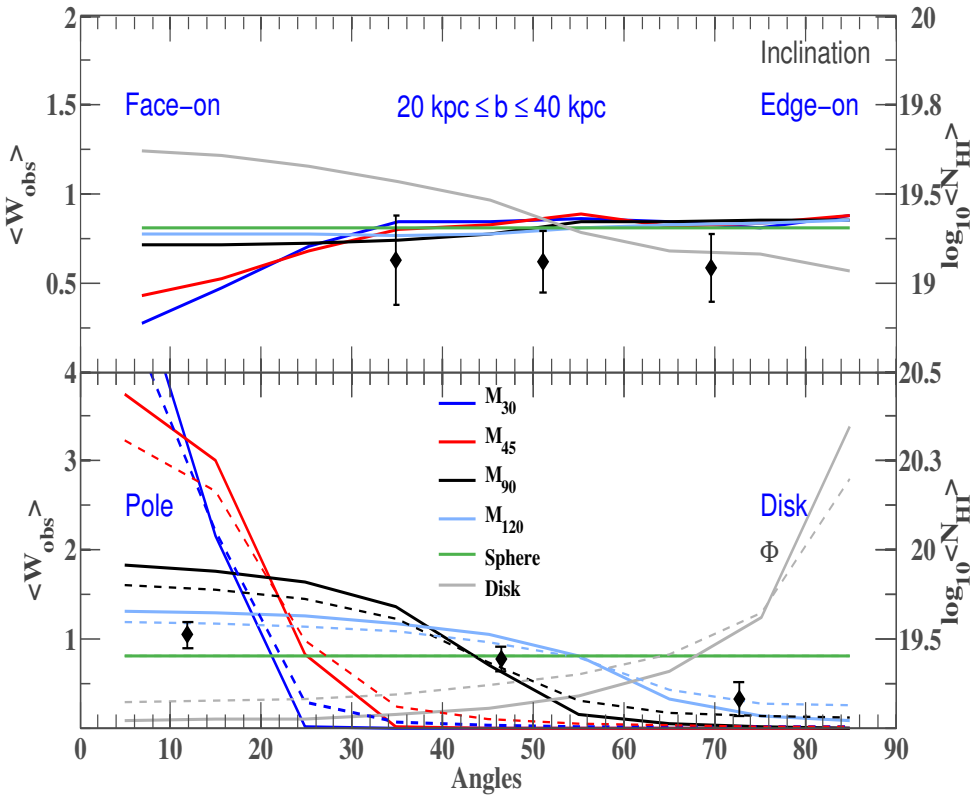

FIG. 4.— The average N_{HI} column density distribution for different models as a function of inclination i (top panel) and azimuth ϕ (bottom panel), both averaged over $20 \leq b \leq 40$ kpc. In the top panel, the i profile is averaged over all ϕ. In the bottom panel, the ϕ profile is averaged over all i (dashed lines) and just over those more highly inclined galaxies with $i \geq 45°$ (solid lines). In all cases we assume that there are no saturation effects. The data points are adopted from the inclination and azimuthal profiles of disk galaxies in Bordoloi et al. (2011)

profile for inclined galaxies ($i \geq 45°$). The sharp bipolar cone models are always stronger along the pole of the galaxy ($\phi \sim 0°$) whereas the disk model exhibits strongest absorption near the plane of the disk ($\phi \sim 90°$). Comparing with the data from Bordoloi et al. (2011), the disk model can be easily ruled out since the azimuthal dependence is of the opposite sign. It should be noted that the curves in figure 4 neglect the effect of saturation which will act to reduce the absorption where it is expected to be strongest (see below). It can be clearly seen from the top panel that the inclination dependence is rather a weak diagnostic of different model geometries and most of the models have essentially the same flat variation with inclination.

It may strike the reader as surprising that there is such a weak dependence on inclination for the 2-d disk model. However, there are two competing effects. The increased sec i path through the disk produces stronger absorption. On the other hand, as shown in equation 6 above, lines of sight (except those that pass through the disk along the line of nodes defined by the plane of the disk and the plane of the sky, i.e. those with $\phi = 90°$ in equation 6) will intersect the disk at progressively larger distances as the inclination of the disk is increased, reducing the absorption. Which of these wins, i.e. the sign of the gradient of the overall $\langle W_{obs} \rangle (i)$ profile, depends on the radial profile of the disk, flatter profiles increase the absorption at high inclinations.

This dependence on radial profile is explored further in Figure 5. All the models in figure 4 have the same value of R_{cut}. We now investigate how the inclination and ϕ dependence vary when R_{cut} is changed. Figure 5 shows the variation in column density as a function of both i and ϕ for the same baseline models if R_{cut} is varied from 25 kpc to 45 kpc. Clearly the ϕ dependence remains much the same and each model can be clearly discriminated. The inclination dependence is much more sensitive to the selection of R_{cut} rendering the discrimination between different models impossible. This plot highlights the fact that azimuthal dependence is a much stronger discriminant for Mg II absorber geometry.

3.2.1. *Effects of line saturation*

All the simulations performed above assume that there is no line saturation and that we are dealing with the linear regime of the curve of growth. This is unlikely to be valid, as discussed in Section 2. Figure 6 shows the inclination and azimuthal dependence for different sets of models after accounting for line saturation using the scheme described in Section 2.

The left panel shows the fiducial models M_{30}, M_{45}, M_{90}, M_{120}, sphere and disk as described above. We also introduce at this point, two hybrid models Hyb1 (M_{90} + sphere) and Hyb2 (M_{90}+ Disk).

The Hyb1 (M_{χ} + sphere) model is constructed by linear combination of a sharp bipolar cone model with opening angle $\chi°$ and the sphere model. The relative strength of the two components is conveniently parametrized as given below,

$$n = \frac{\rho_{cone}}{\rho_{sphere}} \tag{7}$$

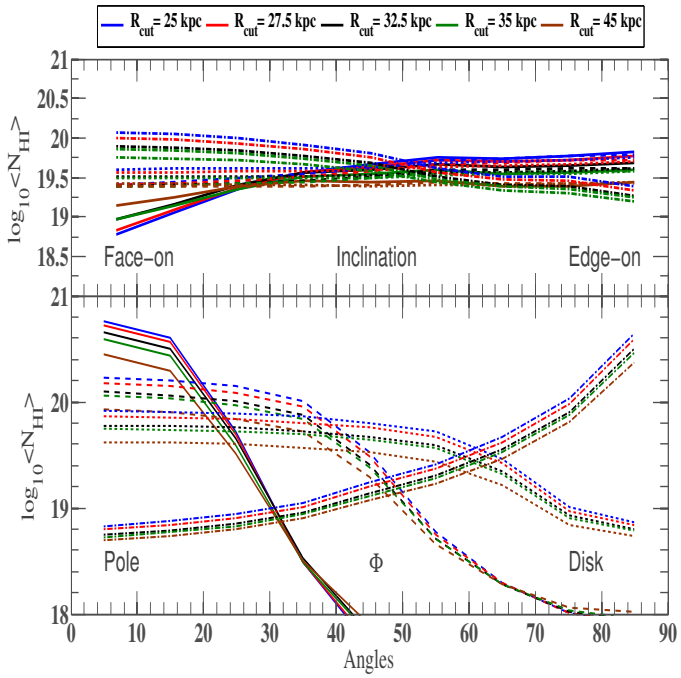

FIG. 5.— The average N_{HI} column density distribution for M_{45} (solid lines), M_{90} (dashed lines), M_{120} (dotted lines) and pure Disk (dot-dashed lines) models which have different radial profiles obtained by setting R_{cut} in the range $25 \leq R_{cut} \leq 45$ kpc, computed as a function of inclination i (top panel) and azimuthal angle ϕ (lower panel). It is noticeable how the sign of the inclination dependence depends on the steepness of the radial profile, because of the two competing effects: the increased path length sec i vs. the effect of sampling greater distances in the disk - see text for discussion. The radial profile has little effect on the azimuthal dependence.

where ρ_{cone} gives the density of neutral hydrogen atoms in the cone region and ρ_{sphere} gives the density of Mg II atoms in the rest of the model. Effectively n gives the over density of neutral hydrogen atoms in the cone region with respect to the rest of the model. n is a free parameter, which can be varied to make the hybrid models have a wide range of density contrast between the cone region and the rest of the model. If $n >> 1$, the cone region dominates the final contribution to the hybrid model. When $n = 1$, the density of atoms in the cone region and the rest of the model is the same and hence irrespective of the opening angle, the hybrid model has a uniform density distribution of a spherical model. If $n < 1$, the number density of atoms in the cone region is less than that in the rest of the model. When $n < 1$, the over density of neutral hydrogen atoms will be aligned along the major axis of the disk. As the opening angle increases, the hybrid model approaches a spherical geometry. The hybrid model is normalized to have the same radial profile as shown in figure 3.

The second hybrid model (Hyb2) is constructed also as a combination of a sharp bipolar cone with opening angle χ and the disk model. The two components of the hybrid model are weighted as defined below

$$W_{hyb} = \frac{f\,W_{cone} + W_{disk}}{1+f} \tag{8}$$

Where W_{hyb} is the contribution to the final hybrid model, W_{cone} is the sharp bipolar cone model with a given opening angle and W_{disk} is the disk model. f is a free parameter which controls the fractional contribution of each of the cone or the sphere/disk component. This hybrid model also has the same radial profile as in figure 3.

Physically, the two hybrid models could represent a scenario where the absorbers originate due to a combination of a bipolar outflow component combined with either a spherical halo component (Hyb1) or an extended disk component (Hyb2). The inclination and radial profiles of these hybrid models are plotted on the left hand panel of figure 6. The right panel of figure 6 shows the same profiles for softened bipolar cone models M_{30}(softened), M_{45}(softened), M_{90}(softened) and M_{120}(softened).

The upper panels of figure 6 show the inclination profiles. As noted above, these show very little variation of absorption strength with inclination i. The bottom panels show the azimuthal profiles. On the left hand set of models, we show only those objects with $i \geq 45°$ since this is where the azimuthal effects are strongest. On the right hand panel (with fewer models) we show both the azimuthal profiles for these inclined objects with $i \geq 45°$(solid lines) and for all inclinations (dashed lines). The hybrid models (left panel) and the softened model (right panel) both well represent the observations. The optimal opening angle and the optimal n and f for these set of models will be determined later in Section 6.

4. APPLICATION TO QUASAR ABSORPTION LINE SYSTEMS

In this section we discuss how the model predictions described above can be translated into observables for a study done with quasar absorption line systems. We show how different models predict the covering fraction distribution for *strong* ($W_r(2796) \geq 0.3$ Å) absorbers, and study the distribution of azimuthal angles (ϕ) of such absorbers in the data from Kacprzak et al. (2011b) and compare them to the expected distribution of different models.

4.1. *Covering Fraction Distribution*

Extended Mg II absorbing gas is seen out to large impact parameters ($b > 100$ kpc) both from quasar absorption line studies and stacked spectra analysis. However both the absorption strength and gas covering fraction declines toward larger radii. Here, we first examine how the gas covering fraction $f(W_{obs} \geq 0.6$ Å) varies with b and W_{obs}.

In the context of our models, the gas covering fraction at an impact parameter b is defined as

$$f(W_{obs} \geq 0.6)(b) = \frac{N_{(W_{obs} \geq 0.6)}(b)}{N_{tot}(b)} \tag{9}$$

$N_{(W_{obs} \geq 0.6)}(b)$ is the number of lines of sight that have an absorber with equivalent width $W_{obs} \geq 0.6$ Å at an impact parameter b and N_{tot} is the total number of lines of sight at the same impact parameter.

Figure 7 shows the covering fraction distribution of $W_{obs} \geq 0.6$ Å absorbers as a function of b for models M_{30}, M_{45}, M_{90}, M_{120}, Sphere, Disk and M_{45}(softened). This plot is similar to a covering fraction distribution of $W_r(2796) \geq 0.3$ Å for a quasar absorption line study. But as the doublet ratio of $W_r(2796) \sim 0.3$ Å systems might be between 1 and 2, there is indeed some leeway in this conversion and comparison. As expected the covering fraction for the Sphere model is a step function with unit covering fraction below and zero covering fraction above $b = 32$ kpc. Although all the sharp bipolar cones have exactly the same average radial profile of total absorption, the covering fractions exhibit a range of radial profiles and approach the spherical case with increasing opening angle. While the disk and the softened bipolar cone models

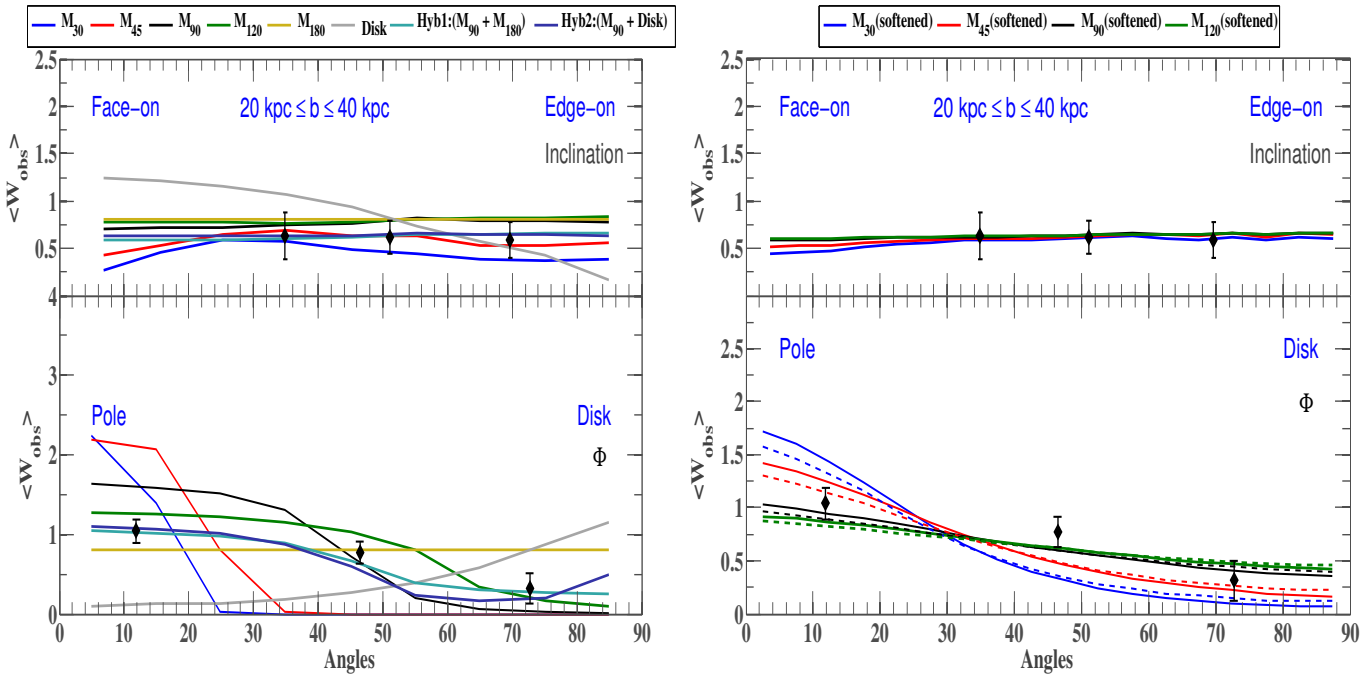

FIG. 6.— The mean $\langle W_{obs} \rangle$ distribution for different models within $20 \leq b \leq 40$ kpc including the effects of the modelled line saturation. The left panels show the sharp bipolar cone models, the sphere, the disk and the hybrid models that are combinations of the M_{90} and the disk or the sphere. The right panels show the softened bipolar cone models. The upper panels show the inclination profile, averaged over all azimuths. The lower panels are inclination-averaged azimuthal profiles. The (solid line) azimuthal profiles in both the left and right lower panels are averaged over i$\geq$ 45°. The dashed lines in the bottom right panel are averaged over all inclinations. The data points are adopted from the inclination and azimuthal profiles of disk galaxies in Bordoloi et al. (2011)

.

exhibit different behavior in detail, it is hard to distinguish between these different geometries purely based on their covering fraction as a function of impact parameter. For all the models, $f(W \geq 0.6) \rightarrow 0$ as $b > 80$ kpc. Observations indicate that the covering fraction does not go to zero as $b > 80$ kpc, for quasar absorption line studies (Nielsen et al. 2012). But the models studied here are for isolated systems and at higher impact parameters contribution from filamentary accretion, satellite galaxies etc will become significant.

Clearly, the radial dependence of covering fraction is not very sensitive to model geometry. The variation of gas covering fractions with inclination and azimuthal angles offer greater discriminatory power. Figure 8 shows the gas covering fraction for $W_{obs} \geq 0.6$ Å absorbers as a function of inclination angle (i) and azimuthal angle (ϕ) within $20 \leq b \leq 50$ kpc. The ϕ dependence of covering fraction is quite obvious from this figure. The sharp bipolar cone models show very high covering fractions near the galaxy pole ($\phi \rightarrow 0$) and which gradually decrease as the cone opening angle increases. They approach the Sphere model as $\chi \sim 180°$. The disk model shows the opposite trend and has a very high covering fraction along the disk axis. The inclination dependence is not as strong as the azimuthal dependence. Only the 2-d disk model exhibits higher covering fraction for the face-on galaxies ($i = 0°$) as compared to the edge-on galaxies ($i = 90°$).

It should be stressed that any comparison of these covering fraction estimates with the observations should be done with care. These covering fraction estimates show how different Mg II absorption distribution geometries manifest themselves in terms of the observed covering fractions relative to each other. The models studied here represent isolated galaxies and the CGM is a more complex environment. These models of isolated systems do not include the effects of filamentary accretion, satellite galaxies or LMC like streams or high velocity clouds (HVCs). Further, we assume a smooth distribution Mg II absorption, and in reality the CGM is more patchy. At high impact parameters these structures will start to contribute significantly to the overall covering fraction. Hence the comparison with the observed covering fraction should be done with these caveats in mind.

4.2. *Distribution of Azimuthal Angles in quasar data*

In this section we discuss the azimuthal dependence of a set of strong ($W_r(2796) \geq 0.3$ Å) Mg II absorbers observed in Kacprzak et al. (2011b). Kacprzak et al. (2011b) had a sample of 40 Mg II absorbing galaxies, out of which 29 have a rest frame equivalent width $W_r(2796) \geq 0.3$ Å. One out of these 29 galaxies is completely face on ($i \leq 5°$) and it becomes rather difficult to assign an accurate azimuthal angle. Hence we exclude this galaxy from our analysis. We shall focus our analysis on this sample of 28 galaxies classified as "strong" absorbers. Galaxy morphology, inclination and azimuthal angles were obtained by using two-dimensional fits of a (co-centered) bulge and disk model. We refer the reader to Kacprzak et al. (2011b) for details of methodology and data reduction details.

Figure 9 shows the distribution of "strong" Mg II absorbers as a function of their azimuthal angle (ϕ) and impact parameter (b). 72% of all the "strong" absorbers (20 out of 28) that are within $b < 120$ kpc lie within 50° of the semi minor axis of the galaxies i.e. to the left of the dashed vertical line of figure 9, as compared with 55% that would be expected for a uniform azimuthal distribution. More significantly, for $b \leq 38$ kpc (below the horizontal dashed line) all of the nine "strong" absorbers lie within 50° of the galaxy semi minor axis. This evidence for a strong azimuthal dependence sup-

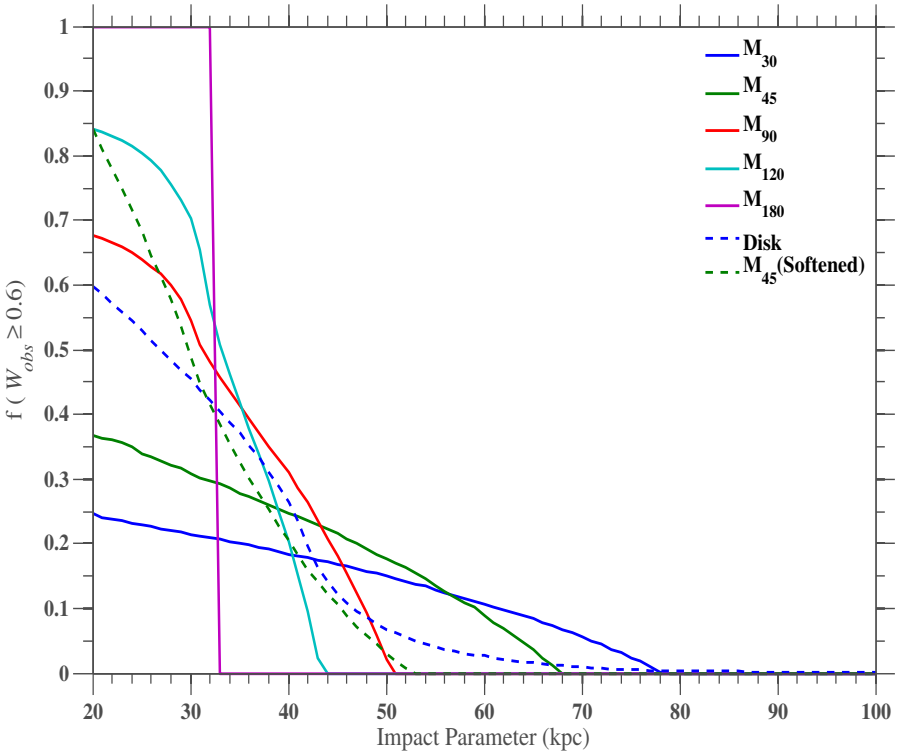

FIG. 7.— The covering fraction for $W_{obs} \geq 0.6$ Å absorbers as a function of impact parameter in different models, all based on idealized smooth 3-d density dtributions. The spherical model shows a step function behavior as expected. The behavior of the sharp bipolar cones vary with opening angle and approach the spherical case with increasing opening angle. The disk and the softened bipolar cone models exhibit different behavior but it is hard to distinguish between different models using this diagnostic.

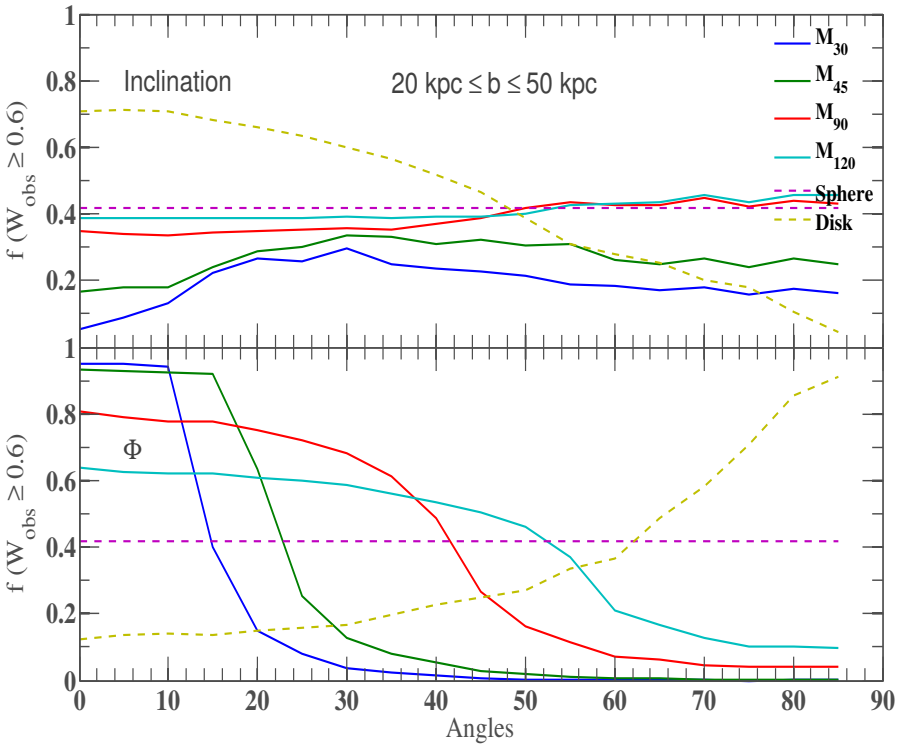

FIG. 8.— Covering fraction for $W_{obs} \geq 0.6$ Å absorbers as a function of i and ϕ for different models. Clearly the azimuthal dependence of covering fraction is a much stronger discriminant of absorber geometry although inclination dependence has a weak correlation with different models.

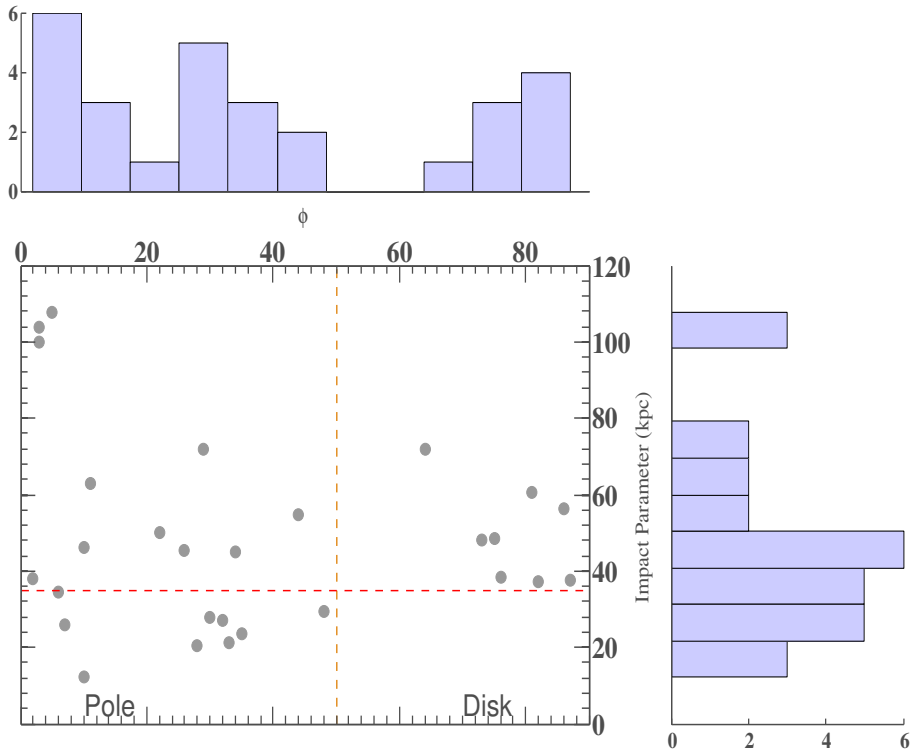

FIG. 9.— The distribution of "strong" Mg II absorbers ($W_r(2796) \geq 0.3$ Å) in azimuthal angle and impact parameter b (adopted from Kacprzak et al. 2011b). 72% of the absorbers lie within 50° of the semi minor axis of the galaxies, i.e. lie to the left of the vertical dashed line. The horizontal dashed line marks $b \leq 38$ kpc. Within this distance, *all* of the absorbers lie within 50° of the semi-minor axis of the galaxy.

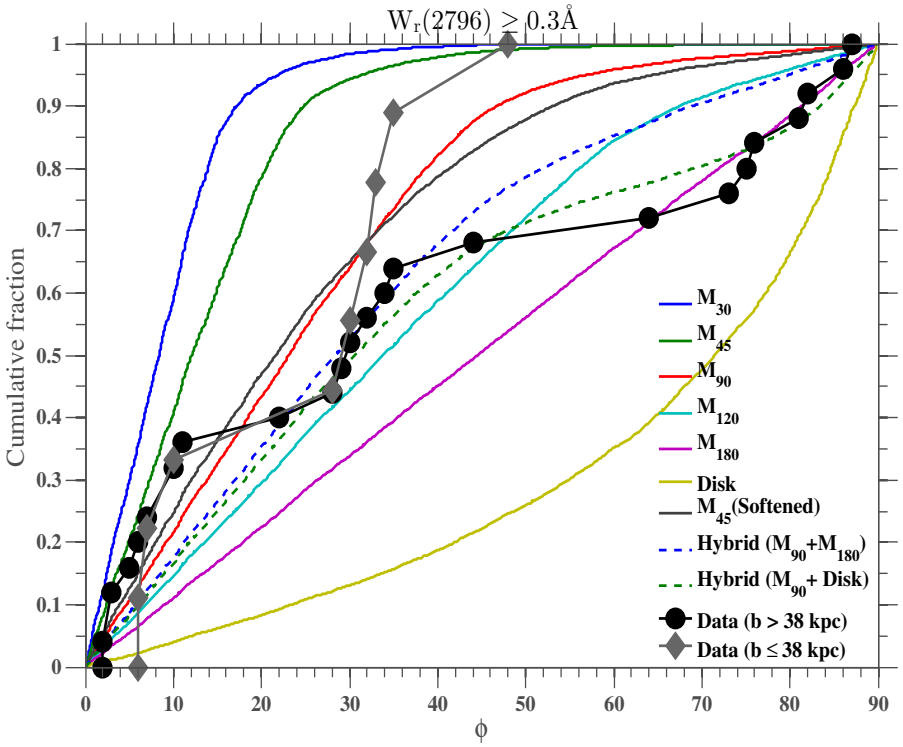

FIG. 10.— Cumulative distribution of azimuthal angles (ϕ) moving away from the projected minor axis for different 3-d models and for the quasar absorption lines with ($W_r(2796) \geq 0.3$ Å, adopted from (Kacprzak et al. 2011b). The data clearly rule out a spherical or a disk-like geometry alone. However a hybrid cone+disk or cone+sphere model or a softened bipolar cone structure is consistent with the data, depending on the opening angle of the cone.

ports the hypothesis that out to $b \sim 40$ kpc the "strong" Mg II absorbers are originating in bipolar galactic winds, as indicated by the measurement of total Mg II absorption in Bordoloi et al. (2011).

To compare this dataset with models we plot the cumulative distribution of ϕ of the Mg II-selected galaxies and a set of models in figure 10. The gray squares represent the cumulative distribution function for the absorbers detected at $b \leq 38$ kpc. Clearly this dataset favors a more cone like distribution of absorbers. The disk and sphere models do not match the data. Even for the absorbers at $b > 38$ kpc (black circles), the quasar absorption line data immediately rule out the disk model. Also M_{30} and M_{45} models do not match the data. The data can however be reproduced by the softened bipolar cone model or a hybrid model. At low impact parameters, the data are consistent with models of small opening angle whereas the high impact parameter data are consistent with high opening angle models. In the next section, we quantify the models supported by the quasar absorption data as well as the integrated spectra data.

5. JOINT ANALYSIS OF STACKED SPECTRA AND QUASAR ABSORPTION LINE SYSTEMS

In this section, we carry out a joint analysis of the two independent and *orthogonal* probes of Mg II absorbers discussed above, namely the stacked spectra data of Bordoloi et al. (2011) and the quasar absorption line probes from Kacprzak et al. (2011b).

We chose a grid of models with opening angles within $1^\circ \leq \chi \leq 170^\circ$ for both the sharp bipolar cone and the softened bipolar cone models. We create, as above, two sets of hybrid models combining a sharp bipolar cone model first with a sphere model and second, with a disk model as described in the previous Section 3.2.1. We examine the cone+sphere hybrid model in the over-density (equation 7) range of $0.1 < n < 10$ and the cone+disk model in the range of $0.1 \leq f \leq 10$ (equation 8). For each model the overall normalization factor α is assigned so that $\langle W_{obs} \rangle \sim 0.7$ Å within $20\ kpc \leq b \leq 50$ kpc.

To compare the models with the integrated spectra data, we compute the mean azimuthal profile for each model within a given bin of impact parameter. The mean azimuthal profiles of the models and the measurements are compared by computing the χ^2 value for each model, taking the minimum χ^2 value as the best fit parameters for each particular set of models.

The quasar absorption line data are compared with the same set of models in the same b bins by performing a two dimensional Kolmogorov-Smirnov test (Peacock 1983; Fasano & Franceschini 1987; Press 2002). To perform the two dimensional Kolmogorov-Smirnov test we chose all "strong" absorbers (above 0.3 Å) within a fixed b range and compare the distribution of inclination and ϕ angles with that expected for different models. Figure 11 shows the distribution of i and ϕ for the"strong" absorbers in six models within $20 \leq b \leq 50$ kpc and the distribution of "strong" absorbers from Kacprzak et al. (2011b). In this b range, the pure (sharp) bipolar cone, sphere and the pure disk models are all ruled out by the 2-D KS test at 5% significance level. The softened bipolar cone, the hybrid cone+sphere and the hybrid cone+disk models are all acceptable (cannot be ruled out) by the 2-D KS test. This reflects the fact that while most of the absorption is above the poles, some significant amount is required at large azimuth angles.

To estimate the model parameters which best represent the observations, we compare the observations with the model predictions within $b \leq 40$ kpc. We first focus on the softened bipolar cone model and compare the models within 20 kpc $\leq$ b $\leq$ 40 kpc with the observations. Figure 12 shows the joint constraints from both the integrated spectra data and the quasar absorption line data. The red curve shows the likelihood curve from the integrated spectra data and the gray hashed region gives the opening angles allowed by the 2-D KS test at 10% significance level (i.e. parameters outside of this region are excluded with more than 90% confidence). The black hashed region is the joint constraints from both these probes which are obtained by simply taking the product of the probabilities. This analysis gives an opening angle of 45^{+15}_{-9} degrees that is allowed by both the observations for a softened bipolar outflow model at 90% confidence.

We now shift our focus on the two hybrid models. We first examine the hybrid model having a cone and a sphere component. As described above we compute the χ^2 values, by comparing each model with the integrated spectra. The allowed confidence contours for the two parameters of interest, n and opening angle are shown in figure 13. The contours show the 68%, 90% and 95% confidence intervals of the allowed model parameters. The blue contours are allowed regions in parameter space obtained from the quasar data at 95% and 90% confidence level. The hashed regions give the joint constraints on opening angle and n at 95% and 90% confidence levels respectively. The left panel shows the allowed model parameters within 20 kpc $\leq$ b $\leq$ 40 kpc. At these impact parameters, both the integrated spectra data and the quasar absorption line data favor models where there is an enhancement of Mg II absorption within $\sim 100^\circ$ of the bipolar region. The opening angle allowed by both the datasets within 40 kpc is $105^{+5\,\circ}_{-10}$ and the over-density n is $2^{+1.3}_{-0.2}$.

We now look at the second hybrid model having a cone and a disk component. Figure 14 shows the constraints on the allowed model parameters, the plotting scheme is the same as described above. The close in data (left panel, 20 kpc $\leq$ b $\leq$ 40 kpc) show that both the quasar absorption line systems and the integrated spectra are in agreement with a cone like geometry with an opening angle of $\sim 110^\circ$. The quasar absorption line data allow for a range of opening angles which are smaller than those allowed by the integrated spectra data. We put joint constraint on the opening angle at $110^\circ \pm 5^\circ$ and the fractional contribution to the cone component is found to be $f = 6^{+4}_{-1}$.

The Mg II absorption around galaxies show strong azimuthal asymmetry for $b < 40$ kpc. But at higher impact parameters, this azimuthal asymmetry is much weaker as shown in Bordoloi et al. (2011). We now investigate the models that can best represent the observations within 41 kpc $\leq$ b $\leq$ 80 kpc as shown in the right panel of figure 13. We see that the models with $n = 1$ i.e. spherical distribution of Mg II gas around the galaxies, cannot be ruled out by either of the datasets. Both the datasets are insensitive to the very low and high opening angles since such very sharp features produce little effect on the overall model. By combining the two probes together we see that the spherically symmetric distribution with $n \sim 1$ is strongly preferred.

Furthermore, the joint models obtained for the two impact parameter ranges at 90% confidence do not overlap. This is evidence that the distribution of Mg II absorbers changes from a highly asymmetric distribution at low impact parameters to a less asymmetric distribution, consistent with a spherical dis-

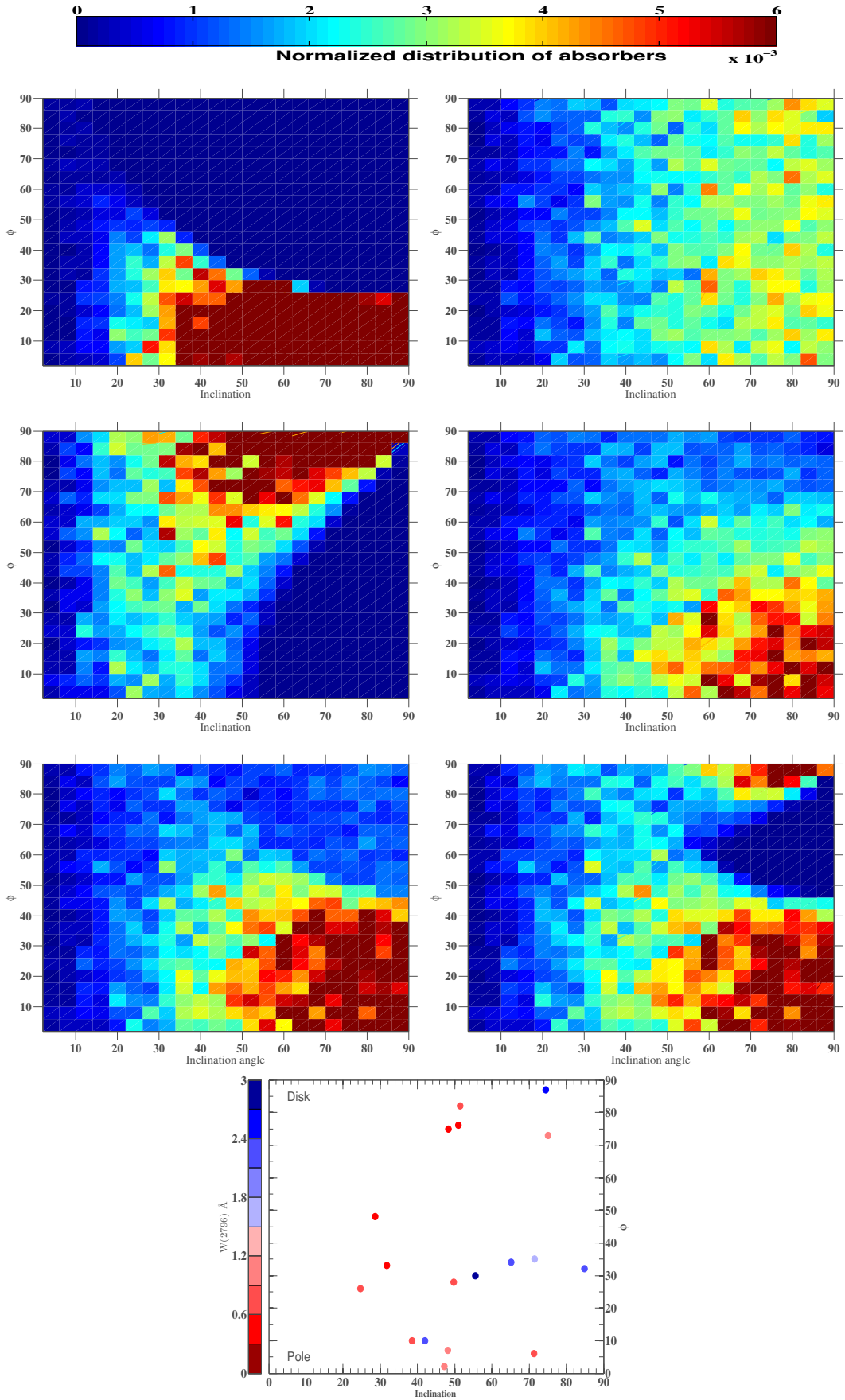

FIG. 11.— The distribution of "strong" Mg II absorbers ($W_r(2796) \geq 0.3$ Å) within $b \leq 50$ kpc as a function of inclination and azimuth. The panel at the bottom shows the data of Kacprzak et al. (2011b). The distribution of strong absorbers in the models with a sharp bipolar cone (M_{45}, top left), with a sphere (top right), a disk (third panel from top), a softened bipolar cone (fourth panel from top), a hybrid cone+sphere (fifth panel from top) and a hybrid cone+disk (sixth panel from top) are also shown. A two dimensional KS test is performed to compare the distribution of absorbers in the models with the observations.

tribution, at high impact parameters.

A similar conclusion is reached from considering the second hybrid model (cone+disk) at the larger impact parameters (right panel, figure 14). The quasar data are quite degenerate in f and opening angle (requiring f to reduce as the opening angle is narrowed) but are consistent with the stacked galaxy analysis. For allowed small opening angles there is significant contribution from the disk component. As the allowed opening angle increases the cone component becomes more and more dominant. Combining these two probes, we get joint constraints on the opening angle = $130^{+40}_{-45}{}^{\circ}$ and $f = 2^{+8}_{-1.1}$. This best fit model also represents an almost spherical geometry with very large opening angle for the cone component. As before, the region allowed at small impact parameters does not overlap with the region allowed at larger radii.

We conclude that the distribution of Mg II gas at low impact parameters is not the same as that found at high impact parameters. This radial trend is hard to see on either the integrated spectra or the quasar absorption line data alone because individually, either probe is not sensitive enough to rule out the same regions of parameter space at different b (figure 13, 14). However the joint analysis reveals that the Mg II gas is distributed preferentially along the minor axis of disk galaxies with an opening angle of $\sim 100^{\circ}$ and an overdensity of $n \sim 2-3$ and $f \sim 6-7$ within $b \leq 40$ kpc. At high impact parameters the distribution is no longer aligned only along the minor axis and a spherical distribution is also consistent with both the dataset.

These models quantify the radial changes in the distribution of Mg II absorbers around galaxies. With the best fit models we can present a more clearer picture of the radial distribution of Mg II absorbing gas. At close impact parameters (e.g. $b \leq 40$ kpc), the Mg II absorption is primarily aligned along the minor axis of the galaxy as they are arising due to material entrained in star formation driven outflows. As we move outwards, the distribution of the absorbers are consistent with either a spherical distribution or a cone with a large opening angle augmented by an extended disk component which might be the signature of in falling material, perhaps as part of a galactic fountain or a contribution from material falling in from larger distances. The more spherical distribution could also reflect the contribution of satellite galaxies.

6. CONCLUSION AND DISCUSSIONS

In this paper we address the principle question of the distribution of cool Mg II gas observed as absorption line systems in the spectra of background sources. We present a suite of 3-dimensional models of Mg II absorption to study the azimuthal and inclination dependence of observational quantities, including the integrated column density and the probability of intersecting a region above a given column density threshold. We compare these model distributions to observations of Mg II absorption that we have previously obtained by stacking the spectra of background galaxies (Bordoloi et al. 2011) and by analyzing, in this paper, the distribution Mg II absorbers in quasar spectra as a function of the impact parameter and relative galaxy orientations (Kacprzak et al. 2011b). Both these *orthogonal* probes of cool ionized Mg II gas, allow us to put joint constraints on the distribution of MgII gas. The main findings of this analysis can be summarized as follows.

1. The azimuthal dependence of the observable quantities is a much stronger diagnostic of the 3-d geometry than the dependence on inclination.

2. A composite model that consists of a simple bipolar cone plus a spherical or disk component or a single softened bipolar distribution can well represent the azimuthal dependencies observed in Bordoloi et al. (2011) at $b < 40$ kpc.

3. The strong Mg II absorbers observed in Kacprzak et al. (2011b) are also asymmetrically distributed. Overall, 72% of these the absorbers are within 50° of the galaxy semi minor axis. Within $b \leq 38$ kpc, "all" the strong absorbers are within 50° of the galaxy semi minor axis. Comparing these absorbers with models and plotting the cumulative distribution of the azimuthal angles, we see that the data is consistent with the distribution of azimuthal angles of bi-polar models and any purely spherical or disk model can ruled out at low impact parameters.

4. A joint analysis combining the integrated spectra data and the quasar absorption line data shows that within 40 kpc both these datasets can be well reproduced by a softened bipolar cone model of opening angle 45^{+15}_{-9} degree or hybrid models consisting of a cone and a sphere component with n is $2^{+1.3}_{-0.2}$ and an opening angle of 105^{+5}_{-10} degree. A second hybrid model with a cone and a disk component is also consistent with the observed data with an opening angle of $110^{\circ} \pm 5^{\circ}$ and $f = 6^{+4}_{-1}$.

5. These analyses show that the Mg II absorbers at low impact parameters are primarily distributed along the minor axis of disk galaxies and are originating in galactic winds, with only a small fraction might be aligned along the major disk axis. In rough terms, the number densities of MgII above the poles of the galaxies are 2-3 times higher than in the planes of the disks.

6. At larger impact parameters ($41\,kpc < b < 80\,kpc$), the distribution of Mg II gas is more symmetric than that observed at smaller impact parameters. A joint analysis of the integrated spectra and the quasar absorption line data shows that the model best representing both the datasets is a more or less spherical distribution of Mg II gas.

7. The clear change in the distribution of Mg II absorption with increasing impact parameter suggests that the origin of the absorption may also change as we move out in radius from the galaxies. The more symmetric distribution at large radii may reflect an increased contribution from in-falling material, or even satellite galaxies.

We also present predictions for the expected covering fraction of strong absorbers as a function of impact parameters for different absorber geometries. The covering fraction as a function of impact parameter is not a strong discriminant of absorber geometry.

We predict the expected inclination and azimuthal dependencies for individual QSO sight lines within 20 kpc $\leq b \leq 50$ kpc for a set of given models. The covering fraction of Mg II absorbers are most sensitive to galaxy azimuthal angles. Amongst the covering fraction profiles, the azimuthal profile of gas covering fraction is the most sensitive probe to discriminate different absorber geometries.

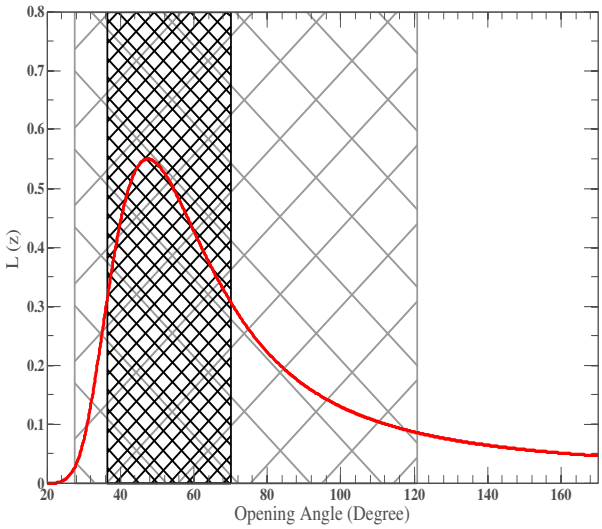

FIG. 12.— The joint constraints on the opening angle of the softened bipolar cone model at $20 < b < 40$ kpc from both the stacked spectra analysis and the quasar absorption line studies. The red solid line is the normalized likelihood curve obtained from the χ^2 minimization of the model predictions to the azimuthal profile in the stacked spectra analysis. The maximum likelihood opening angle of about 45° is consistent with the opening angles allowed by performing a 2D KS test of the model angle distributions with the quasar absorption line data (shown as the open hashed region). The close hatched region shows the joint constraint at 90% confidence level.

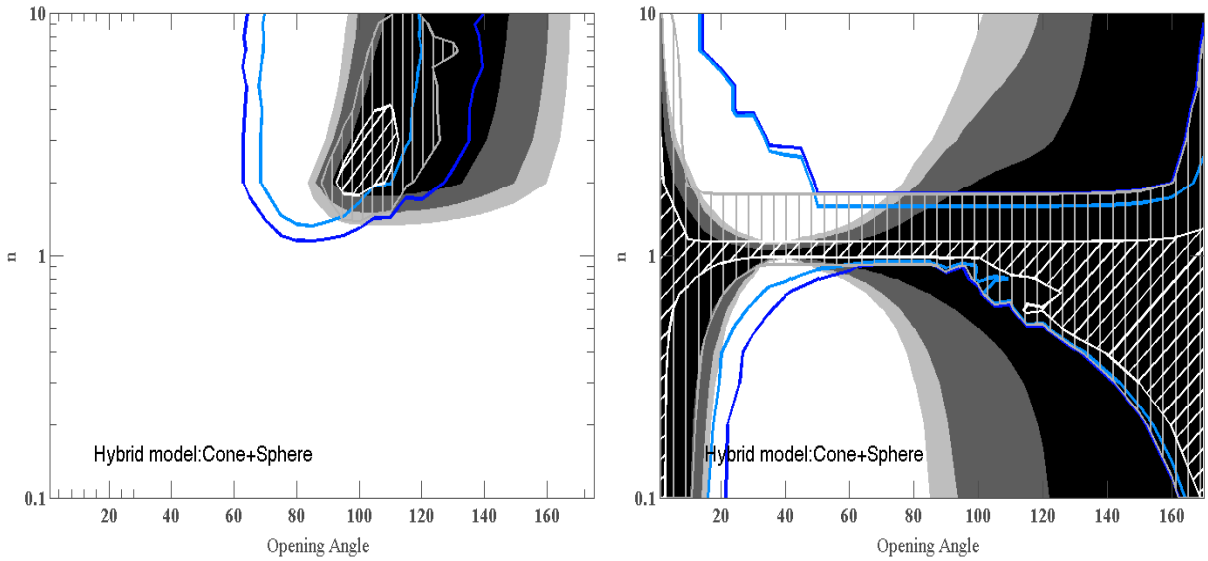

FIG. 13.— Joint constraints on the hybrid Cone+Sphere model from both stacked spectra analysis and the quasar absorption line studies on two parameters describing this model - these are n, the density contrast above the pole and in the plane of the disk, and the cone opening angle. The 68%, 90% and 95% confidence contours obtained from χ^2 fitting of the model predictions to the azimuthal profile in the stacked spectra analysis (gray contours). The blue contours show the parameter space allowed by the quasar absorption line data at 90% and 95% confidence level, obtained from a 2D KS test analysis. The hashed region on both panels show the parameter space allowed by both datasets at 90% and 95% confidence level. The left panel is for absorption within $20\,kpc \leq b \leq 40\,kpc$, and the right panel is for absorption within $40\,kpc \leq b \leq 80\,kpc$. The differences show the pronounced weakening of the azimuthal asymmetries with radius.

This work has been supported by the Swiss National Science Foundation. We also acknowledge useful discussions with Nicolas Bouché.

REFERENCES

Bergeron, J. & Stasińska, G. 1986, Astronomy and Astrophysics, 169, 1
Bordoloi, R., et al. 2011, The Astrophysical Journal, 743, 10
Bouche, N., Hohensee, W., Vargas, R., Kacprzak, G. G., Martin, C. L., Cooke, J., & Churchill, C. W. 2011, ArXiv e-prints:1110.5877
Bouché, N., Murphy, M. T., Péroux, C., Csabai, I., & Wild, V. 2006, MNRAS, 371, 495
Charlton, J. C. & Churchill, C. W. 1998, ApJ, 499, 181
Charlton, J. C., Ding, J., Zonak, S. G., Churchill, C. W., Bond, N. A., & Rigby, J. R. 2003, ApJ, 589, 111
Chen, H., Helsby, J. E., Gauthier, J., Shectman, S. A., Thompson, I. B., & Tinker, J. L. 2010, ApJ, 714, 1521
Churchill, C. W., Kacprzak, G. G., Nielsen, N. M., Steidel, C. C., & Murphy, M. T. 2012, ApJ, submitted
Churchill, C. W., Kacprzak, G. G., & Steidel, C. C. 2005, Proceedings of the International Astronomical Union, 1, 24
Churchill, C. W., Mellon, R. R., Charlton, J. C., Jannuzi, B. T., Kirhakos, S., Steidel, C. C., & Schneider, D. P. 2000, ApJS, 130, 91
Fasano, G. & Franceschini, A. 1987, MNRAS, 225, 155

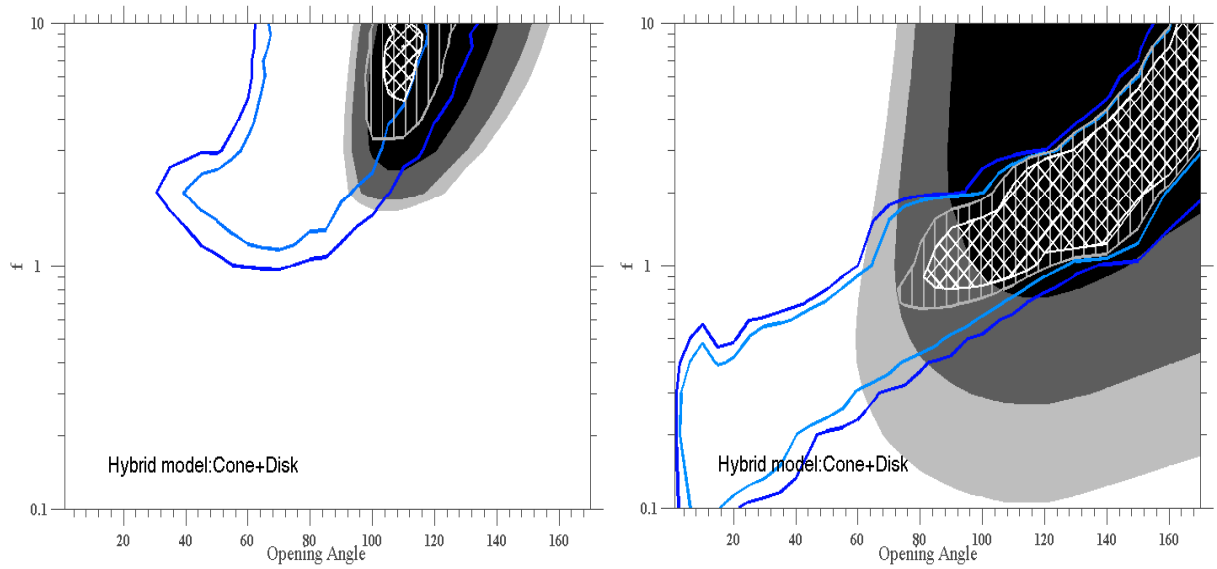

FIG. 14.— As in Figure 13, but for the hybrid Cone+Disk model. The parameters are now f, the ratio of the total amount of material in the cone to the disk, and the cone opening angle.

Fujita, A., Martin, C. L., Mac Low, M.-M., New, K. C. B., & Weaver, R. 2009, ApJ, 698, 693

Heckman, T. M. 2002, in Astronomical Society of the Pacific Conference Series, Vol. 254, Extragalactic Gas at Low Redshift, ed. J. S. Mulchaey & J. T. Stocke, 292

Kacprzak, G. G., Churchill, C. W., Barton, E. J., & Cooke, J. 2011a, ApJ, 733, 105

Kacprzak, G. G., Churchill, C. W., Evans, J. L., Murphy, M. T., & Steidel, C. C. 2011b, MNRAS, 416, 3118

Kacprzak, G. G., Churchill, C. W., & Nielsen, N. M. 2012, ArXiv e-prints:-1205.0245

Kacprzak, G. G., Churchill, C. W., Steidel, C. C., & Murphy, M. T. 2008, Astronomical Journal, 135, 922

Lanzetta, K. M., Turnshek, D. A., & Wolfe, A. M. 1987, ApJ, 322, 739

Lilly, S. J., et al. 2007, ApJS, 172, 70

Martin, C. L., Shapley, A. E., Coil, A. L., Kornei, K. A., Bundy, K., Weiner, B. J., Noeske, K. G., & Schiminovich, D. 2012, ArXiv e-prints:-1206.5552

Ménard, B. & Chelouche, D. 2009, MNRAS, 393, 808

Nestor, D. B., Turnshek, D. A., & Rao, S. M. 2005, ApJ, 628, 637

Nielsen, N. M., Churchill, C. W., & Kacprzak, G. G. 2012, ArXiv e-prints:-1211.1380

Oppenheimer, B. D., Davé, R., Kereš, D., Fardal, M., Katz, N., Kollmeier, J. A., & Weinberg, D. H. 2010, MNRAS, 406, 2325

Peacock, J. A. 1983, MNRAS, 202, 615

Petitjean, P. & Bergeron, J. 1990, Astronomy and Astrophysics, 231, 309

Press, W. H. 2002, Numerical recipes in C++ : the art of scientific computing

Prochaska, J. X., Kasen, D., & Rubin, K. 2011, ApJ, 734, 24

Prochter, G. E., Prochaska, J. X., & Burles, S. M. 2006, ApJ, 639, 766

Rao, S. M., Turnshek, D. A., & Nestor, D. B. 2006, ApJ, 636, 610

Rigby, J. R., Charlton, J. C., & Churchill, C. W. 2002, ApJ, 565, 743

Rubin, K. H. R., Prochaska, J. X., Koo, D. C., & Phillips, A. C. 2012, ApJL, 747, L26

Rubin, K. H. R., Weiner, B. J., Koo, D. C., Martin, C. L., Prochaska, J. X., Coil, A. L., & Newman, J. A. 2010, ApJ, 719, 1503

Sargent, W. L. W., Steidel, C. C., & Boksenberg, A. 1988, ApJ, 334, 22

Steidel, C. C. 1995, in QSO Absorption Lines, ed. G. Meylan, 139

Steidel, C. C. & Sargent, W. L. W. 1992, ApJS, 80, 1

Veilleux, S., Cecil, G., & Bland-Hawthorn, J. 2005, Annual Review of Astronomy and Astrophysics, 43, 769

Weiner, B. J., et al. 2009, ApJ, 692, 187